Applied Science and Engineering Progress, Vol. 20, No. 2, 2027, 8254

Research Article

Metallurgical Analysis and Economic Feasibility of Thermite Welding Applied to Railway Rail Surface Repair

Thongchai Khrueaphue
Program of Industrial Engineering Technology and Logistics, Faculty of Agricultural and Industrial Technology, Phetchabun Rajabhat University, 67000, Thailand

Parinyawatr Dhinnabutra*
Faculty of Technical Education, Rajamangala University of Technology Isan, Khon Kaen, 40000, Thailand

Charoenchai Ridtirud
Department of Civil Engineering, Faculty of Engineering, Rajamangala University of Technology Isan, Khon Kaen, 40000, Thailand

Narong Srihajong
Department of Mechanical Engineering, Faculty of Engineering, Rajamangala University of Technology Isan, Khon Kaen Campus, 40000, Thailand

Saksit Chuenchomnakjad
Department of Industrial Education, Faculty of Engineering, Rajamangala University of Technology Lanna Phitsanulok, 65000, Thailand

* Corresponding author. E-mail: Parinyawat.ti@rmuti.ac.th, DOI: 10.14416/j.asep.2026.07.011
Received: 11 April 2026; Revised: 24 May 2026; Accepted: 15 June 2026; Published online: 23 July 2026

Abstract

This study developed welding molds and investigated the metallurgical behavior of thermite repair welds for R260 grade railway rail surface repair using a Mixture Design approach, together with an economic feasibility analysis in comparison with conventional welding. Mold compressive strength increased significantly with slica sand content (p-value < 0.01), while graphite and water exerted negative effects on strength (p-value < 0.05) and increased porosity through a significant interaction effect. With thermal resistance ranged from 1,430 to 1,570 °C, Runs 1, 2, and 6 provided the best balance of properties, with all models demonstrating high accuracy ($R^2 > 0.90$). Mold Type 1 produced rough weld surfaces with slag residue and numerous pores, while Mold Type 2 produced smoother surfaces with minimal porosity and no cracks, neither mold type exhibited macro-level cracking. SEM analysis revealed that the base metal consisted of lamellar pearlite ($\alpha + Fe_3C$). Mold Type 1 produced coarse pearlite with grain boundary ferrite and significant pore accumulation, whereas Mold Type 2 yielded fine, uniform pearlite with virtually no porosity. EDX analysis indicated micro-segregation in Mold Type 1 welds, suggesting structural non-uniformity and potential stress concentration sites, while Mold Type 2 welds exhibited more uniform elemental distribution, which may promote fine pearlite formation and defect reduction. Economic analysis showed that thermite welding costs 290 THB per joint versus 960 THB for SMAW (Cost Ratio, CR = 3.31; cost savings of 69.8%), and requires only 15–20 minutes compared to 90 minutes (Time Reduction Ratio, TRR = 4.5), suggesting promising economic feasibility under the conditions evaluated. The hardness test results showed that Mold Type 2 provided uniform hardness values, with HAZ hardness ranging from 360–410 HV and weld zone hardness ranging from 320–360 HV. These results were consistent with the SEM and EDX analyses, which revealed a fine pearlitic microstructure and homogeneous elemental distribution, indicating that Mold Type 2 was more suitable for railway rail surface repair than Mold Type 1.

Keywords: Economic feasibility, R260 grade railway, Rail surface repair, Thermite welding, Thermal resistance

Applied Science and Engineering Progress, Vol. 20, No. 2, 2027, 8254

1 Introduction

Railway rails are critical components of railway transportation systems, playing a direct role in operational safety and transportation efficiency. In particular, 100-pound-per-yard steel rails continue to be widely utilized throughout Thailand's railway network because they represent a standard rail type suitable for the load capacity and operating speeds of major railway lines. Although these rails possess high mechanical strength, they are highly susceptible to fatigue damage and surface wear at the rail head during long-term service. Therefore, appropriate repair and maintenance procedures are essential for extending rail service life and reducing the costs associated with rail replacement [1]-[3]. In addition, surface defects occurring on the rail head significantly influence the metallurgical structure and long-term performance of the rail material.

At present, railway rail surface repair is commonly performed using conventional welding processes such as Shielded Metal Arc Welding (SMAW) and hardfacing techniques. However, these methods still exhibit several limitations, including the requirement for highly skilled welders, prolonged repair time, and limited applicability in remote areas where electrical power is unavailable. These constraints increase operational complexity and overall maintenance costs, particularly when railway traffic interruptions are required during repair operations [1], [4]. In contrast, thermit welding is a joining technique based on the highly exothermic reduction reaction between aluminum and iron oxide, capable of generating temperatures exceeding 2,500 °C and producing complete metal fusion within a short period of time [5]. This process has considerable potential for improving metallurgical continuity between the repaired region and the original rail material while minimizing microstructural imperfections commonly associated with conventional repair methods. Furthermore, thermit welding offers significant economic advantages because it does not require an external power supply or large-scale equipment, making it highly suitable for field operations, especially in remote locations [6], [7].

Nevertheless, the application of thermit welding specifically for "rail surface repair" remains limited and requires further investigation. Surface defects on railway rails are generally localized and shallow, which significantly affect heat accumulation, heat distribution, and cooling rate during the welding process. These factors directly influence the resulting microstructure, including grain size, phase distribution, and the formation of the Heat Affected Zone (HAZ) [8], [9]. Therefore, investigating the effects of welding process parameters on metallurgical characteristics, such as weld phase formation and HAZ morphology, is critically important for evaluating weld quality and structural reliability. Accordingly, this research focuses on investigating the metallurgical characteristics, mechanical properties, and economic feasibility associated with the application of thermit welding technology for railway rail surface repair. The study also includes a comparative cost analysis between thermit welding and conventional repair methods to establish new scientific knowledge regarding thermit-based rail surface repair technology. The findings of this research are expected to contribute to the development of a highly efficient, cost-effective, and practically applicable railway maintenance approach that can be sustainably implemented under real field conditions [3], [7], [10].

2 Materials and Methods

2.1 *Welding mold*

2.1.1 Experimental design

The design and fabrication of welding molds for thermite rail surface repair involved developing a new prototype mold, distinct from conventional thermite welding molds that accommodate large volumes of molten metal and withstand the metallostatic pressure of molten metal and high thermal loading. This study focused on identifying an appropriate material formulation for mold fabrication to achieve physical properties capable of withstanding high temperatures, providing adequate strength, and preventing cracking during use [4], [11]. In the experimental design, silica sand was set in the range of 80–90% as the principal structural component; bentonite clay served as a natural clay binder providing green (pre-cure) strength during compaction; graphite powder enhanced thermal resistance; sodium silicate served as a chemical binder activated by CO_2 curing to develop final bond strength; and Water controlled workability during mixing.

Subsequently, a Design of Experiments (DOE) approach was employed to enhance experimental efficiency [12], minimize unnecessary trial runs, and improve the capability of mold design optimization. A total of 10 experimental runs were generated based on the D-optimal Mixture Design principle [13], which is an effective statistical technique for selecting material compositions that appropriately cover the design space with maximum efficiency. Each experimental run was assigned different material proportions in order to investigate the influence of composition on the properties of the mold, as presented in Table 1. During the experiments, materials were accurately weighed and blended under controlled conditions (constant mixing time, temperature, and environment). After specimen preparation, material properties, including compressive strength, porosity, and thermal resistance, were tested in triplicate to enhance data reliability. Data were analyzed using analysis of variance (ANOVA) to assess variable significance, and a Scheffé polynomial model was fitted to describe the relationship between composition and response [14].

The fundamental principle of this study's experimental design was based on Mixture Design, whose basic constraint requires that the sum of all component proportions equals 1 (or 100%), as expressed in Eq. (1):

$$\sum_{i=1}^{5} X_i = 1 \quad (1)$$

Or, in the specific form of this study, as expressed in Eq. (2):

$$X_1 + X_2 + X_3 + X_4 + X_5 = 1 \quad (2)$$

where:
X_1 = Silica Sand
X_2 = Bentonite Clay
X_3 = Graphite Powder
X_4 = Sodium Silicate Solution
X_5 = Water

The model used in this study is the Scheffé polynomial model, a specific form of Mixture Design, expressed in general form as Eq. (3):

$$\hat{y} = \sum_{i=1}^{5} \beta_i X_i + \sum_{i=1}^{4} \sum_{j=i+1}^{5} \beta_{ij} X_i X_j \quad (3)$$

where $\hat{y}$ is the predicted response, X_i and X_j are the coded proportions of the mixture components, β_i is the linear coefficient, β_{ij} is the binary interaction coefficient, and i and j are component indices for the five mixture components, with $i < j$.

This model was developed by considering the mixture sum constraint and therefore contains no intercept term, enabling it to appropriately describe the behavior of the mixture system.

2.1.2 Mold design and fabrication

Mold design and fabrication are critical steps in the thermite welding process. As shown in Figure 1(a) and Figure 1(d) (Mold Type 1), the mold was designed with a central pouring hole for the molten metal, enabling it to flow into the weld zone uniformly from all directions. Riser vents on the side were also incorporated to expel air and excess metal from the mold, thereby reducing the formation of gas pockets or voids within the weld and producing a dense, high-

Table 1: Material composition ratios for welding mold fabrication.

Run	Silica Sand (%)	Bentonite Clay (%)	Graphite (%)	Sodium Silicate Solution (%)	Water (%)
1	90	3	2	3	2
2	88	4	3	3	2
3	85	5	3	4	3
4	83	6	4	4	3
5	80	7	5	5	3
6	87	5	2	4	2
7	84	6	3	4	3
8	82	7	4	4	3
9	86	4	4	3	3
10	83	5	5	4	3

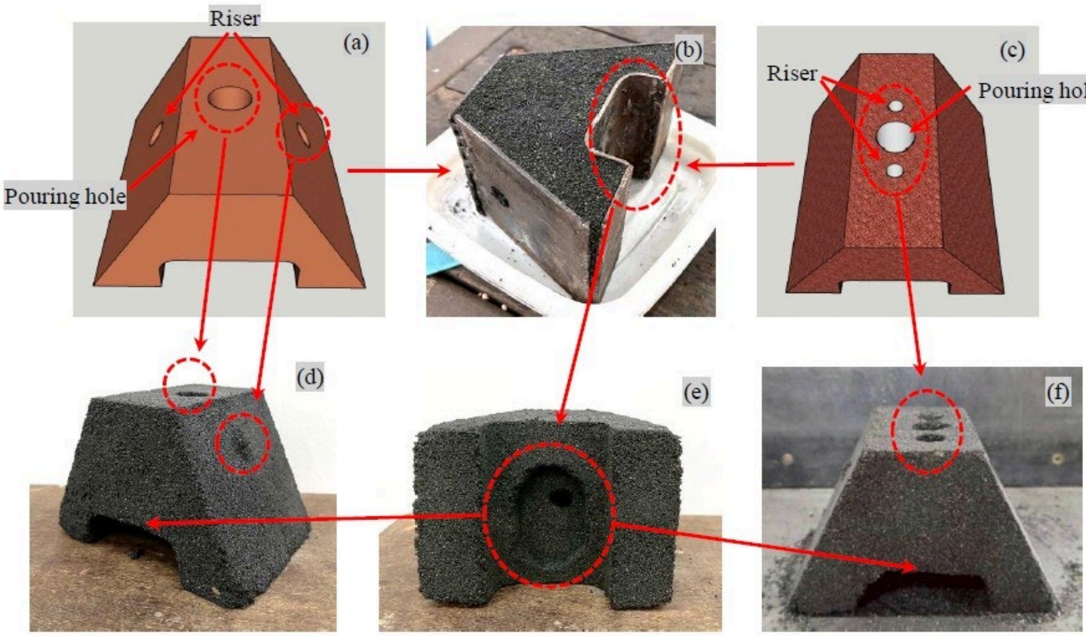

Figure 1: Mold design and fabrication, (a) mold type 1 design, (b) metal fabrication form, (c) mold type 2 design, (d) fabricated mold type 1, (e) bottom concave profile and (f) fabricated mold type 2.

quality weld [15]. Figure 1(b) and Figure 1(e) show the mold fabrication step, in which sand mixed with a sodium silicate binder was compacted into a specific form. The base of the mold was designed with a concave profile to receive molten metal poured during welding. This concave shape facilitates metal pooling without splashing, promotes uniform heat distribution, and produces a weld with the correct form and adequate strength [16]. As shown in Figure 1(c) and Figure 1(f) (Mold Type 2), an alternative mold design was developed, also featuring a central pouring hole but with overflow vents repositioned to the top of the mold. This design was intended to allow trapped air to be expelled upward and excess metal to overflow through the top vents, thereby reducing air-void formation and improving weld density. After mold fabrication, carbon dioxide (CO_2) gas was purged into the mold interior to accelerate hardening. The CO_2 reacts chemically with the sodium silicate binder, causing rapid mold hardening without the need for drying. Prior to use, the molds were cured in an oven at 250 °C for 1 hour.

2.1.3 Thermite crucible fabrication

Thermite crucible design and fabrication are critical steps in the thermite welding process for railway rail surface repair, as a specialized application to achieve weld quality and operational safety. The thermite crucible serves as a vessel for thermite powder, which undergoes a high-temperature exothermic redox reaction during welding; the crucible design and materials must therefore withstand high temperatures and control molten metal flow appropriately [17-20]. As shown in Figure 2(a), the crucible was designed as a cylindrical vessel lined internally with mold material approximately 10 mm thick, which was sufficient to withstand the heat of the thermite reaction and was subsequently CO_2-hardened. A Ø10 mm outlet was left at the base of the crucible (Figure 2(b)) to allow continuous, accurately directed molten metal flow into the welding mold. Approximately 350 g of thermite powder was then loaded, and the crucible was sealed tightly (Figure 2(c)) to prevent moisture ingress and atmospheric contamination, which could otherwise affect reaction initiation and performance.

2.2 *Rail steel and thermite powder*

The rail steel used in this study was R260 Grade (100 lb/yard type), a material conforming to EN 13674-1:2003 [21], [22], currently in use by the State Railway of Thailand, owing to its well-balanced

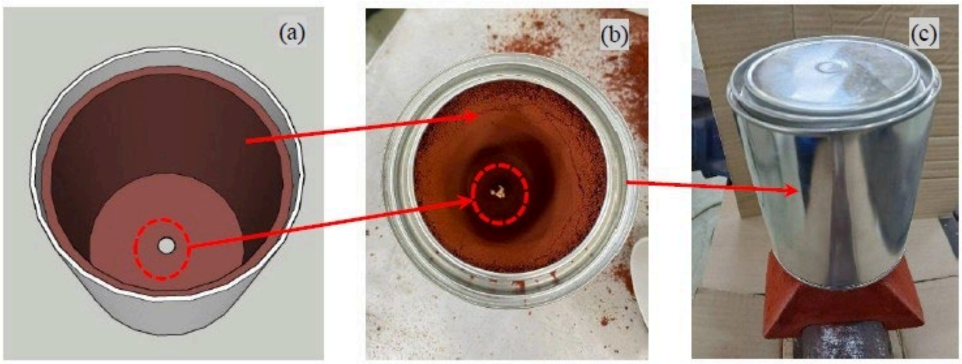

Figure 2: Thermite crucible fabrication, (a) schematic cross-section of crucible, (b) top-view photograph of the fabricated crucible and (c) crucible charged.

mechanical properties of strength, toughness, and wear resistance [23], [24]. To simulate actual service wear conditions, specimens were prepared by machining a simulated wear groove measuring is (top) overview of the wear zone (dashed circle); (bottom left) close-up view showing groove dimensions of 65 mm (length) × 40 mm (width); (bottom right) groove depth of 5 mm measured using a welding gauge, confirming the reference dimensions used for machining simulated wear grooves on test specimens (Figure 3), referencing average damage dimensions observed during actual field operations. Prior to welding, the groove surface was ground and dressed to the designed dimensions to accommodate molten metal accumulation and thermal loading during welding. The chemical composition of the R260 rail steel used in the experiments is shown in Table 2 [21], [22], which indicates the proportions of alloying elements Mn and Si contributing to strength and wear resistance, together with controlled P, S, and H levels that are important for toughness, weld integrity, and resistance to hydrogen-related cracking during long-term rail service [25], [26].

Figure 3: Surface wear groove on an in-service R260 grade.

Thermite powder (Table 3) was used as the principal heat-generating medium in the thermite welding process, exploiting an oxidation–reduction (redox) reaction between iron oxide (Fe_2O_3) and aluminum powder (Al), which yields molten iron and alumina slag (Al_2O_3) while releasing heat at temperatures of approximately 2,500–3,000 °C sufficient to melt and fuse the base metal effectively [1], [27], [28]. This reaction can be expressed according to Eq. (4), in which iron oxide acts as the oxidizing agent and aluminum as the reducing agent:

$$Fe_2O_3 + 2Al \rightarrow 2Fe + Al_2O_3 + Heat \quad (4)$$

The chemical composition of the thermite powder used in this study is shown in Table 3, which indicates the reactant proportions affecting chemical properties and the quantity of thermal energy generated during the welding process.

2.3 *Thermite welding procedure for rail surface repair*

This study investigated thermite welding for railway rail surface repair using two mold configurations, Mold Type 1, shown in Figure 4(a), with riser vents on the side, and Mold Type 2, shown in Figure 4(e), with overflow vents repositioned to the top. Welding was then conducted to examine the metallurgical properties of the resulting weld deposits. Both mold types had undergone preliminary evaluation under multiple welding factors and were found to produce acceptable weld surface characteristics and were therefore selected for in-depth analysis.

The welding procedure began with preheating the specimen using an oxy-acetylene torch, as shown

Table 2: Chemical composition of R260 grade railway rail steel.

Grade (EN 13674-1)	Fe	C (%)	Mn (%)	Si (%)	P (%)	S (%)	H (ppm)
R260	Balance	0.60–0.82	0.65–1.25	0.13–0.60	≤ 0.030	≤ 0.025	≤ 2.5

Table 3: Chemical composition of thermite powder (by weight).

Specification	Fe_2O_3 (%)	Al (%)	Mn, C, Si, Cr, Ni (%)	MgO/CaO (%)	BaO, CaF_2 (%)
Thermite Powder (Manufacturer spec.)	Balance (~70–75)	20–25	1–3	≤ 1	≤ 1

Note: Composition values represent typical ranges per manufacturer specification, with Fe_2O_3 constituting the balance. Minor variations exist between batches; EN 14730-1:2006 (Aluminothermic Welding of Rails) was used as the reference standard for aluminothermic welding material requirements [1], [27], [28]

in Figure 4(b). In the thermite rail surface repair process, the specimen was preheated to approximately 800–850 °C for 5 minutes, as measured by a thermocouple. This preheating temperature was intentionally selected to compensate for heat loss during mold assembly, thermite crucible installation, and thermite ignition procedures. During these preparation stages, the specimen temperature gradually decreased to approximately 700 °C before the actual melting process began. Therefore, the effective welding temperature was maintained close to the limit recommended by EN 14730-1, helping to reduce the risk of excessive austenite grain growth. In addition, preheating allowed the rail surface temperature to approach the melting temperature, which improved weld penetration and reduced residual stress during the welding process. [25], [30], [31]. The welding mold and thermite crucible were then assembled onto the rail as shown in Figure 4(f), and the thermite powder was ignited through the ignition port at the top of the crucible, initiating the oxidation–reduction reaction to generate temperatures in excess of approximately 2,500 °C. Molten metal from the thermite reaction flowed into the mold to fill the worn rail surface area, as shown in Figure 4(c) and Figure 4(d) for Mold Type 1 (side riser vents) and Figure 4(g) for Mold Type 2 (top overflow vents). After the molten metal had solidified, the mold was removed and the weld surface was ground flush with the original rail profile.

3 Results and Discussion

3.1 *Mold properties*

Mold specimens were fabricated as 50-mm cubes and tested for compressive strength according to ASTM C109/C109M-21 (Standard Test Method for Compressive Strength of Hydraulic Cement Mortars Using 2-in. or 50 mm Cube Specimens), which was adopted as the most applicable standard for the silica sand sodium silicate binder system used in this study [32]. The measured mold properties for all ten experimental runs are presented in Table 4. The results demonstrated that mold properties, including compressive strength, porosity, and thermal resistance, varied systematically with composition, consistent with the Mixture Design principle in which all variables are interrelated under the 100% sum constraint. Compressive strength was positively correlated with Silica Sand content: Run 1 (2.36 MPa, 90% Silica Sand) produced the maximum compressive strength, while Run 5 (1.56 MPa, 80% Silica Sand) produced the minimum, confirming Silica Sand as the principal factor with high significance (p-value < 0.01). Conversely, Graphite and Water exerted negative effects on strength (p-value < 0.05). Porosity increased from 11.5% to 19.0% as Graphite and Water contents increased, particularly in Runs 5, 8, and 10, indicating a significant interaction effect (X_3X_5, p-value < 0.05). Thermal resistance was positively correlated with Silica Sand and Graphite contents: Run 1 yielded the maximum of 1,570 °C and Run 5 the minimum of 1,430 °C, consistent with the ANOVA results confirming the statistical significance of both variables (p-value < 0.05). Overall, a clear property trade-off was observed; formulations with high strength also showed low porosity and high thermal resistance (e.g. Run 1), while formulations with higher Graphite and Water contents exhibited

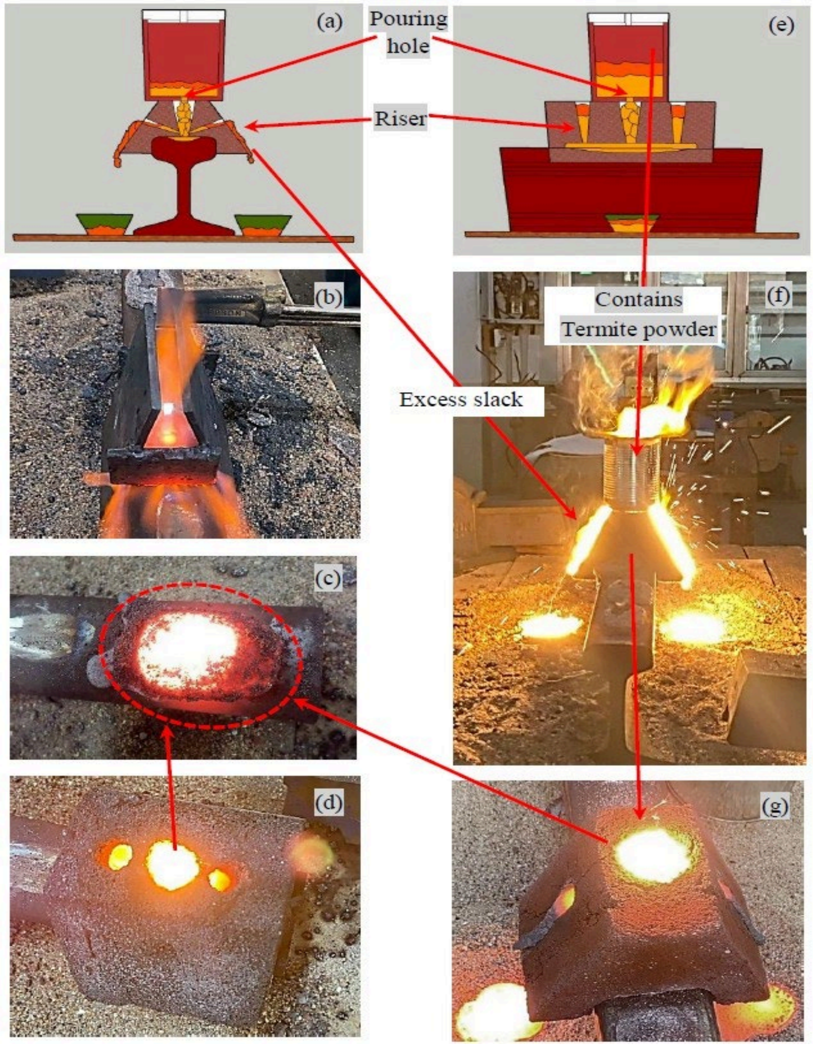

Figure 4: Thermite welding procedure for rail surface repair, (a) and (e) schematic cross-sections showing crucible and mold assembly, (b) preheating of the rail specimen, (c) and (g) molten metal filling the simulated wear groove, (d) and (f) thermite reaction and molten metal discharge through riser vents.

increased porosity and reduced strength. Runs 1, 2, and 6 provided the best balance of properties. All fitted models were statistically appropriate ($R^2 > 0.90$, with non-significant lack-of-fit not significant) and can therefore be used effectively for predicting and designing optimal compositions for practical use. The full range of mold properties and the threshold values defining optimal formulation performance are summarized [1], [31], in Table 5.

3.2 *Weld surface inspection and macrostructure*

Both mold types successfully filled the simulated wear groove with molten metal. As illustrated in Figure 5(a), Mold Type 1 produced a rough weld surface with slag residue, as indicated by the arrows, and numerous surface pores; however, no visible surface cracking was detected [33]. In contrast, Figure 5(b) shows that Mold Type 2 produced a noticeably smoother upper weld surface, with only minor porosity and no visible cracks. Although upward discharge through the top vents was not fully smooth, causing part of the molten metal to spread outward near the mold base, the overall weld surface quality was improved compared with Mold Type 1. Macrostructural examination of the transverse section, shown in Figure 5(c), clearly distinguished the upper weld zone (Up WZ), lower weld zone

Table 4: Mold properties from D-optimal Mixture Design experiments.

Run	Compressive Strength (MPa)	Porosity (%)	Thermal Resistance (°C)	Remark
1	2.36	11.5	1,570	Optimal a)
2	2.17	13.5	1,540	Optimal a)
3	1.80	15.0	1,505	
4	1.63	17.0	1,470	
5	1.56	19.0	1,430	Lowest performance b)
6	1.96	12.5	1,535	Optimal a)
7	1.77	16.0	1,490	
8	1.56	18.0	1,455	
9	1.88	16.5	1,510	
10	1.64	17.5	1,475	

Note: a) Optimal: formulation achieving the most favorable combination of high compressive strength (≥ 1.96 MPa), low porosity (≤ 13.5%), and high thermal resistance (≥ 1,535 °C) based on ANOVA results ($R^2 > 0.90$), b) Lowest performance: formulation exhibiting the lowest compressive strength (1.56 MPa) and thermal resistance (1,430 °C) with the highest porosity (19.0%).

Table 5: Summary of mold property ranges and optimal formulation performance.

Property	Min (Run 5)	Max (Run 1)	Optimal Runs (1, 2, and 6)	Significance
Compressive Strength (MPa)	1.56	2.36	≥ 1.96	p-value < 0.01
Porosity (%)	19.0	11.5	≤ 13.5	p-value < 0.05
Thermal Resistance (°C)	1,430	1,570	≥ 1,535	p-value < 0.05

Note: Significance levels determined by ANOVA with Scheffé polynomial model ($R^2 > 0.90$, lack-of-fit not significant for all responses).

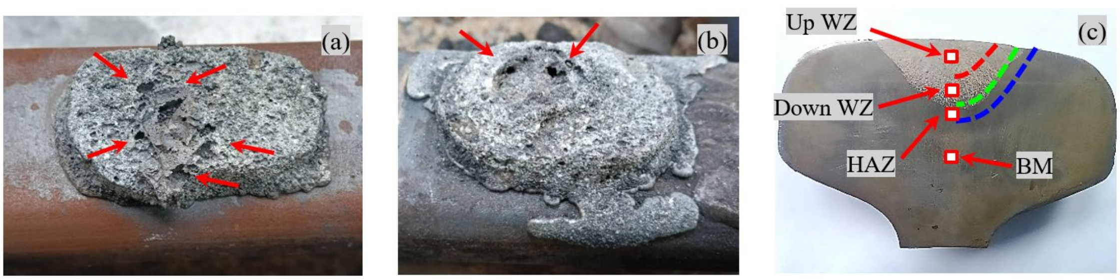

Figure 5: Weld surface morphology and macrostructural examination, (a) Mold Type 1, (b) Mold Type 2 and (c) transverse cross-section of the thermite weld repair.

(Down WZ), and heat-affected zone (HAZ), with no macro-scale cracking or large internal pores evident. Similar HAZ microstructural modification has also been reported in thermite-welded rail steels [1], [34].

3.3 *Microstructural analysis*

3.3.1 SEM examination

SEM microstructural analysis (Figure 6(a)) revealed that the base metal (BM) of R260 grade rail steel consisted of lamellar pearlite ($\alpha + Fe_3C$) with uniform alternating layers of ferrite (α) and cementite (Fe_3C), with only minor grain boundary ferrite detected. Cooling rate and heat transfer behavior also played significant roles in the microstructural evolution of thermite welds, particularly in influencing pearlite lamellar spacing. The results indicated that Mold Type 1 tended to promote localized heat accumulation,

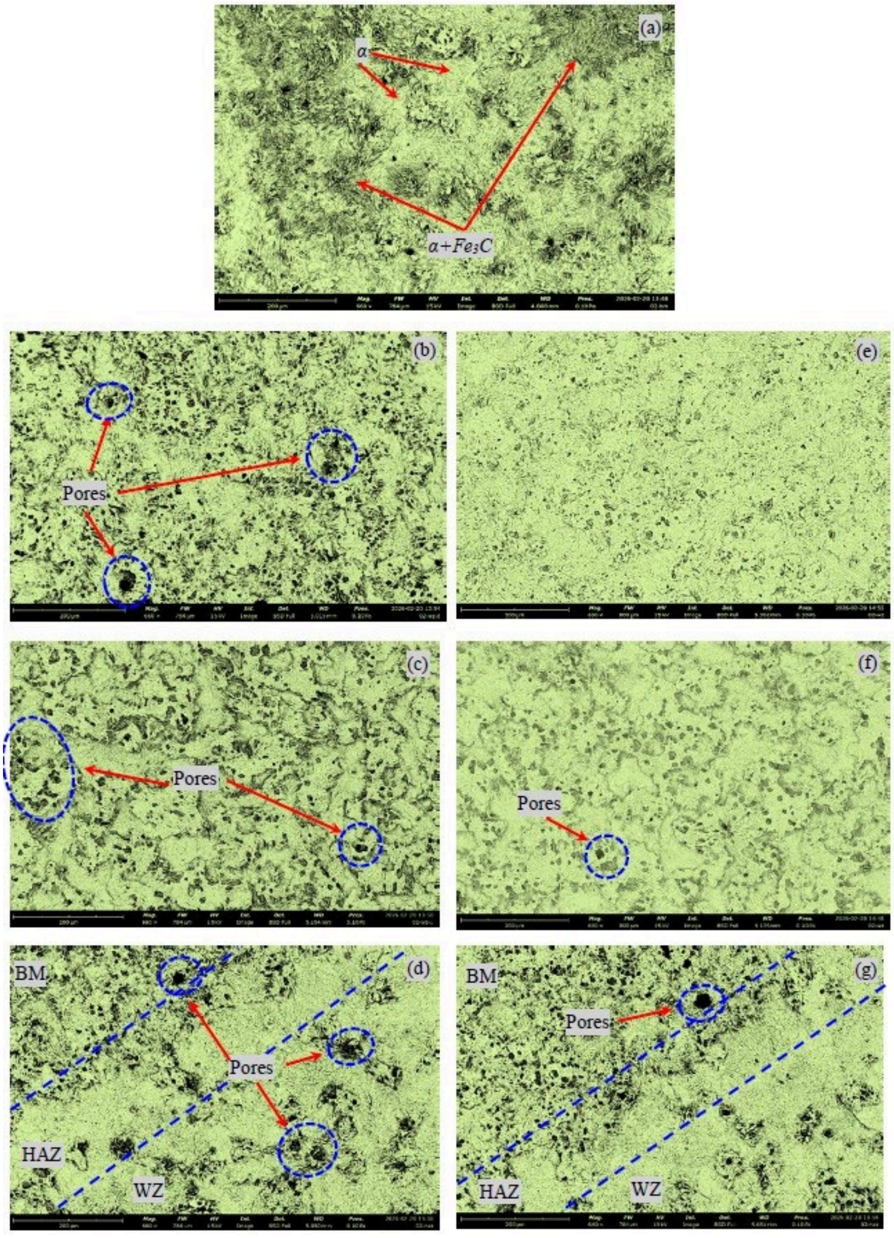

Figure 6: SEM micrographs of R260 rail steel base metal and thermite weld zone microstructures, (a) base metal (BM), Mold Type 1 (b) upper weld zone, (c) lower weld zone, (d) HAZ of Mold Type 1 and Mold Type 2 (e) upper weld zone, (f) lower weld zone, (g) HAZ of Mold Type 2.

which may be associated with its side-vent design, resulting in the formation of coarse pearlite, grain boundary ferrite, and substantial porosity. In contrast, Mold Type 2 exhibited more uniform heat distribution and heat transfer behavior, leading to the formation of fine and densely distributed pearlite, reduced porosity, and a more continuous hardness profile.

Microstructural examination of Mold Type 1 (Figure 6(b)–6(d)) showed that the upper weld zone (Figure 6(B)) exhibited prior austenite grain growth, resulting from heat accumulation and slow cooling, producing coarse pearlite together with numerous pores. The lower weld zone (Figure 6(c)), as the region of maximum heat accumulation, displayed pearlite with wide lamellar spacing and minor porosity. The HAZ (Figure 6(d)) showed coarse pearlite with grain boundary ferrite and significant pore accumulation [35], which may act as crack initiation sites under actual service loading.

Microstructural examination of Mold Type 2 (Figure 6(e)–6(g)) demonstrated markedly improved microstructure compared to Mold Type 1. The upper weld zone (Fig. 6(e)) showed fine, densely laminated pearlite, which may contribute to improved hardness and deformation resistance, with no porosity or cracks detected [36], [37]. The lower weld zone (Figure 6(f)), despite high heat exposure, maintained fine, uniform lamellar pearlite, suggesting well-controlled cooling conditions. The HAZ (Figure 6(g)) showed only minor structural change, retaining a fine-grained character expected to support material toughness and strength. These results indicate that Mold Type 2 provides better microstructural control than Mold Type 1, suggesting potential improvement in mechanical reliability and serviceability of the rail repair weld under the tested conditions.

3.3.2 EDX elemental analysis

EDX analysis of the weld zone in Mold Type 1 (Figure 7) revealed that the weld metal primarily comprised Fe (90.49 wt.%), along with C (6.11 wt.%), Si (1.80 wt.%), and Mn (1.30 wt.%). It should be noted that EDX results indicate general elemental trends, and carbon values in particular should be interpreted qualitatively due to the inherent limitations of EDX in quantifying light elements. Examination of elemental distribution showed that Mn and Fe tended to cluster locally in some regions, while Si distributed separately, indicating micro-segregation at the microscopic level during weld metal solidification [33]. The detected carbon content suggests a tendency toward

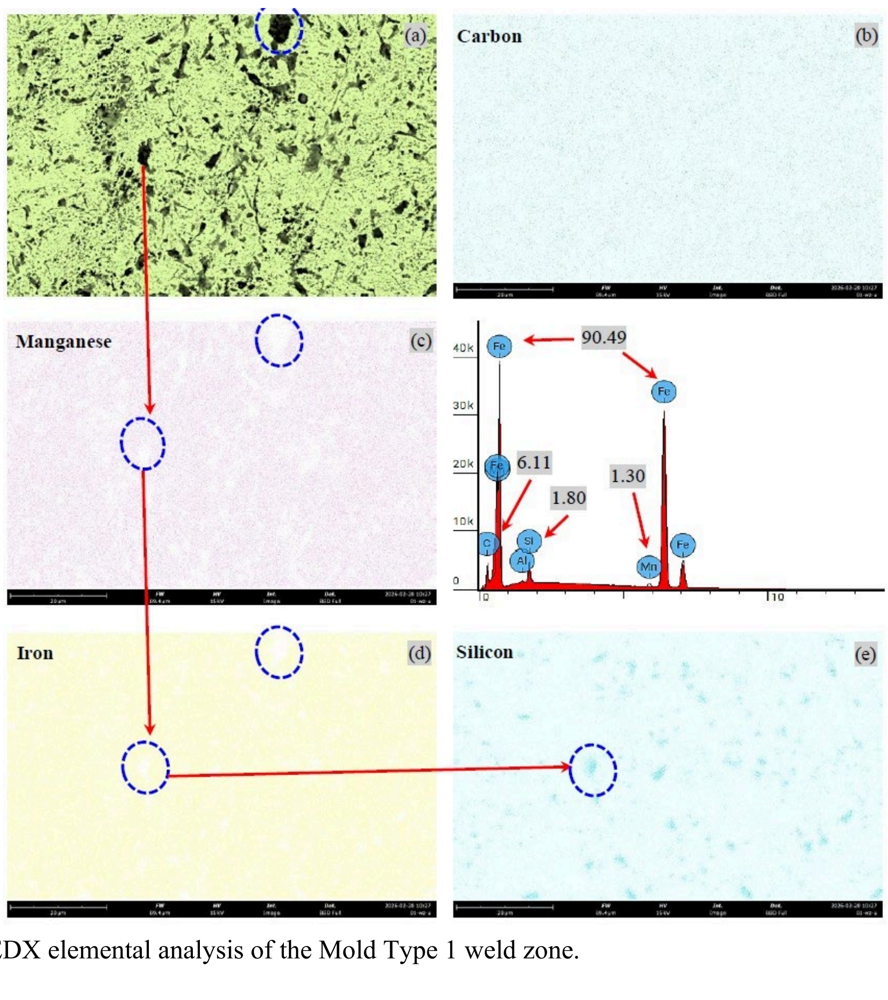

Figure 7: EDX elemental analysis of the Mold Type 1 weld zone.

carbide phase (Fe_3C) formation. Manganese (1.30 wt.%) may contribute to strength enhancement; however, non-uniform distribution of Mn and its separation from Si may create regions of specific composition, causing microstructural discontinuity. This compositional non-uniformity may lead to stress concentration sites [38] and, combined with the porosity observed in SEM, is expected to increase the risk of crack initiation under cyclic loading, potentially affecting weld performance in rail surface repair applications.

EDX analysis of the weld zone in Mold Type 2 (Figure 8) revealed that the weld metal primarily comprised Fe (86.80 wt.%), along with C (11.30 wt.%), Mn (1.30 wt.%), and Si (0.50 wt.%). As with Mold Type 1, carbon values should be interpreted qualitatively. Examination of elemental distribution at the microscopic level showed that all elements were distributed uniformly with no clustering or phase segregation. The detected carbon content suggests a tendency toward carbide phase (Fe_3C) formation, which may promote the formation of a fine pearlite structure and is expected to contribute to improved hardness and wear resistance. The uniform elemental distribution and homogeneous element partitioning suggest a more continuous microstructure, potentially reducing stress concentration sites and minimizing internal defects, which is consistent with the fine pearlite microstructure observed in the SEM analysis. These characteristics are expected to enhance fatigue resistance [38] and tribological performance under service conditions. The compositional analysis of Mold Type 2 therefore suggests a promising metallurgical advantage over Mold Type 1, with its uniform elemental distribution potentially contributing to improved mechanical properties and service life of rail repair welds. Further mechanical testing is recommended to confirm these trends.

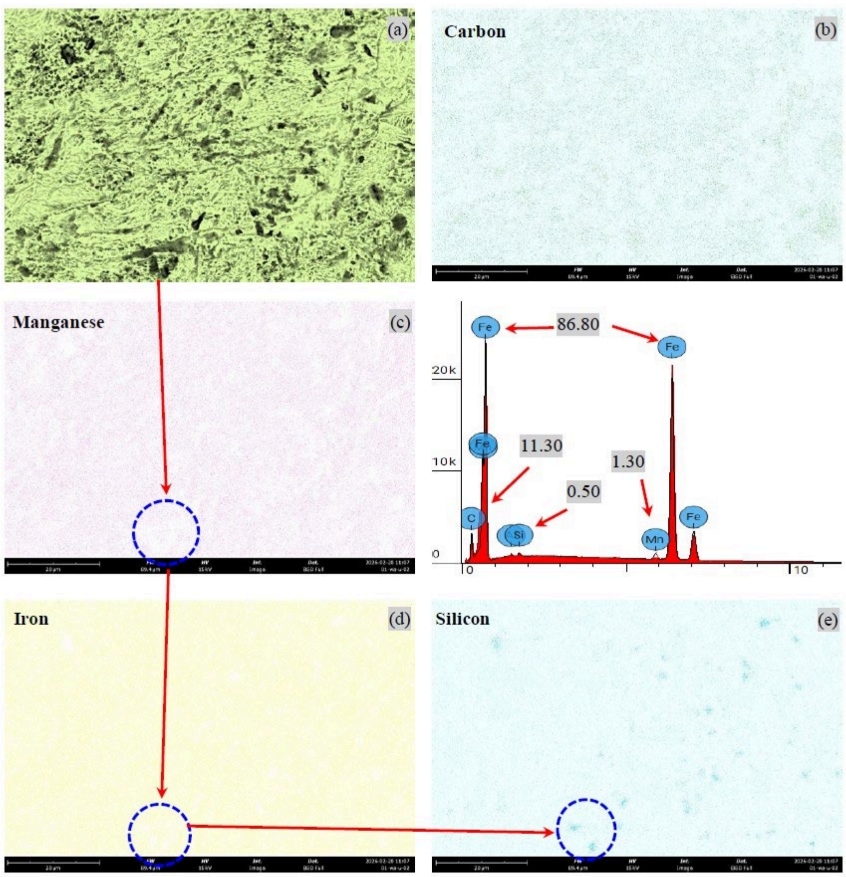

Figure 8: EDX elemental analysis of the Mold Type 2 weld zone.

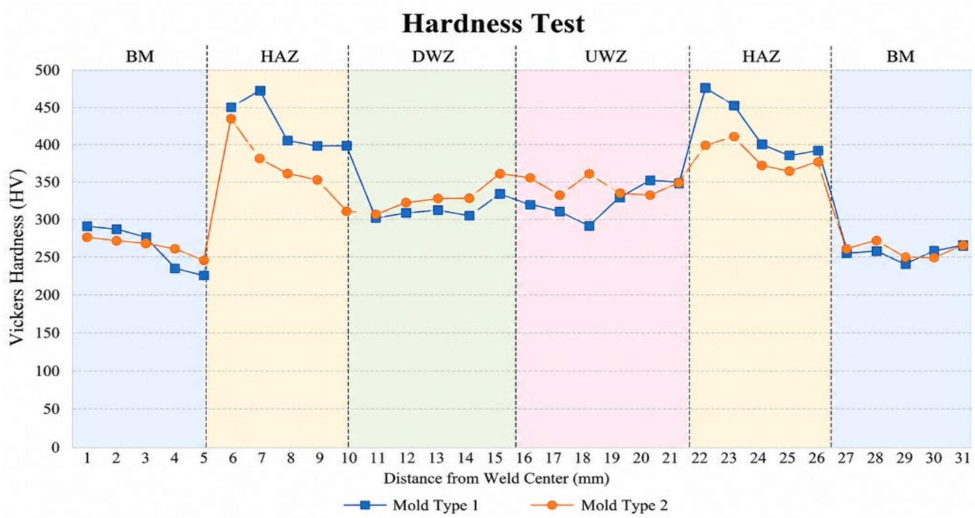

Figure 9: Hardness distribution in railway rail surface repair welds.

3.4 *Hardness test results*

Figure 9 presents the Vickers hardness distribution measured using the HV10 method, corresponding to a test force of 98.1 N (10 kgf) and an indentation dwell time of 10 s, together with the SEM and EDX analyses. The combined results demonstrate that the Mold Type 2 design provided more suitable weld characteristics for railway rail surface repair applications. This improvement is attributed to the formation of a fine pearlitic microstructure and a more uniform elemental distribution, particularly Fe, Mn, and Si, resulting in a more continuous hardness profile and hardness values closer to those of the original rail material. In the base metal (BM) region, both mold conditions exhibited comparable hardness values within the range of approximately 245–280 HV, which is consistent with the mechanical property range generally reported for pearlitic rails and thermit-welded rail systems [39].

However, significant differences were observed in the heat-affected zone (HAZ). Mold Type 1 exhibited considerably higher and more fluctuating hardness values, ranging from approximately 395 to 476 HV, which were substantially greater than those of the original rail material. This behaviour suggests a non-uniform thermal history and local microstructural variation, primarily associated with coarse pearlite formation and elemental segregation. Such hardness fluctuation may increase local brittleness and elevate the risk of crack initiation under cyclic loading conditions during actual service. Similar variations in mechanical properties across thermit-welded rail regions have also been reported in previous studies [39], [40].

In contrast, Mold Type 2 exhibited HAZ hardness values within the range of approximately 360–410 HV, with a more gradual and continuous hardness transition. Furthermore, both the upper weld zone (UWZ) and lower weld zone (DWZ) showed relatively uniform hardness values in the range of approximately 320–360 HV, indicating more stable thermal and solidification conditions. These findings are consistent with the SEM and EDX results, which revealed a fine pearlitic structure and a homogeneous elemental distribution throughout the weld region. Such metallurgical characteristics may reduce local hardness mismatch and stress concentration tendency, thereby improving the structural reliability and service performance of the repaired railway rail [39]–[41].

3.5 *Economic analysis*

The comparative economic analysis between thermite welding and SMAW hardfacing (Table 6) demonstrated that thermite welding offered significant advantages in terms of cost, time, and operational efficiency under the conditions evaluated. The average total cost per repair joint for thermite welding was only 290 THB, compared with 960 THB for SMAW hardfacing, representing a difference of 670 THB per joint, or approximately 69.8% savings. Furthermore, thermite welding required only up to 20 minutes per repair joint,

Table 6: Economic comparison between thermite welding and SMAW hardfacing.

Parameter	Thermite Welding	SMAW Hardfacing
Material	Thermite powder 350 g @ 400 THB/kg = 140 THB/joint	Flux-coated electrode ~1 kg @ 550 THB/kg = 550 THB/joint
Labor	No highly skilled welder required; avg. 150 THB/joint	Certified skilled welder required; avg. 350 THB/joint
Repair time per joint	~15–20 minutes total	~90 minutes total
Energy	No electricity / no fuel required	Generator: 1.5 L fuel × 40 THB = 60 THB/joint
Equipment	Mold, small gas cylinder, grinder	Welding machine, small gas cylinder, generator, grinder
Portability	Lightweight; easy to move; usable in confined areas	Heavy; difficult; requires trolley/additional labor
Safety	Safe from electric shock, heat	Risk of electric shock, heat, flux spatter, radiation
Weld quality	Good penetration; no cracking; low porosity	Multi-pass required; flux inclusion risk; stress; cracking and porosity
Rail downtime	Short; rail can resume service quickly	Long closure required
Total cost/joint	Material 140 + Labor 150 = 290 THB/joint	Material 550 + Labor 350 + Fuel 60 = 960 THB/joint
Throughput per 8-hr shift	24 joints (480 ÷ 20 minutes)	5–6 joints (480 ÷ 90 minutes)

versus 90 minutes for SMAW hardfacing, representing a 77.8% reduction in working time, or 4.5 times the throughput within an equivalent time period [38], [42].

In terms of energy and equipment requirements, thermite welding requires no electrical power supply, relying instead on an oxy-acetylene torch for preheating and the self-sustaining thermite reaction for metal fusion. This makes the process highly suitable for confined or remote locations where electrical infrastructure is unavailable, whereas SMAW hardfacing requires a generator, fuel, and gas cylinders, thereby increasing energy costs and transportation complexity. Thermite welding also reduces the opportunity cost associated with rail closure, requiring only 20 minutes per joint compared with 90 minutes for SMAW. It significantly reduces traffic suspension and improves operational service efficiency [42].

This study uses a simplified cost comparison approach based on direct material, labor, and energy costs under field-representative conditions. Economic performance was quantified using two indices. First, the Cost Ratio (CR), defined in Eq. (5), was calculated as the ratio of the reference method cost to the proposed method cost:

$$CR = Creference / Cproposed \quad (5)$$

where $C_{reference}$ = 960 THB/joint (SMAW) and $C_{proposed}$ = 290 THB/joint (Thermite welding).

$$CR = 960 / 290 = 3.31$$

A CR > 1 indicates that thermite welding is less costly per repair joint. A CR of 3.31 suggests that thermite welding may offer a unit cost reduction of approximately 69.8% relative to SMAW hardfacing under the conditions evaluated. Second, the Time Reduction Ratio (TRR) is defined in Eq. (6):

$$TRR = T_{reference} / T_{proposed} = 90 / 20 = 4.5 \quad (6)$$

Under the conditions evaluated, thermite welding required approximately 4.5 times less time per repair joint and showed 69.8% lower cost than SMAW hardfacing. Together, CR = 3.31 and TRR = 4.5 suggest that thermite welding demonstrates promising economic performance across both cost and time dimensions. These findings indicate that thermite welding may offer promising economic feasibility and operational efficiency for field rail maintenance in Thailand, particularly for applications requiring reduced cost, time, and energy. However, a comprehensive lifecycle cost analysis is recommended for broader economic validation [43].

3.6 *Limitations*

This study is limited to laboratory-scale experiments focusing on localized rail surface repair under controlled conditions. Mechanical performance properties such as hardness, wear resistance, and fatigue behavior were not directly evaluated in this study and should be addressed in future work using standardized testing methods. In addition, EDX analysis was employed for qualitative elemental assessment only; the detected carbon values in particular should not be used for quantitative phase determination. Further characterization techniques such as X-ray diffraction (XRD) are recommended for phase confirmation. The economic analysis presented is based on a simplified cost comparison using direct material, labor, and energy costs, and does not account for lifecycle costs, equipment depreciation, or indirect operational factors. Field validation under actual service conditions is also recommended before full-scale implementation.

4 Conclusions

Mold properties varied significantly with composition. Compressive strength was primarily governed by Silica Sand content (p-value < 0.01), while Graphite and Water reduced strength and increased porosity through a significant interaction effect (p-value < 0.05). Optimal formulations (Runs 1, 2, and 6) achieved compressive strength ≥ 1.96 MPa, porosity ≤ 13.5%, and thermal resistance ≥ 1,535 °C, with all fitted models demonstrating high predictive accuracy ($R^2 > 0.90$). Weld surface and defects, Mold Type 1 produced rough surfaces with slag residue and numerous pores, although no macro-level cracks were detected, these pores may act as potential damage initiation sites. Mold Type 2 produced smoother surfaces with lower porosity and no cracks, reflecting more appropriate metal flow and solidification behavior under the tested conditions.

The base metal microstructure consisted of pearlite ($\alpha + Fe_3C$). In the weld zone, Mold Type 1 produced coarse pearlite grains with wide lamellar spacing, grain boundary ferrite, and substantial pore accumulation. In contrast, Mold Type 2 weld zones exhibited fine, densely laminated, and uniform pearlite grains with virtually no porosity, suggesting improved microstructural characteristics compared with Mold Type 1.

EDX elemental analysis indicated general elemental trends in the weld metal. Mold Type 1 (Fe 90.49 wt.%, C 6.11 wt.%, Si 1.80 wt.%, Mn 1.30 wt.%) showed signs of micro-segregation, with Mn and Fe clustering and causing compositional non-uniformity. Mold Type 2 (Fe 86.80 wt.%, C 11.30 wt.%, Mn 1.30 wt.%, Si 0.50 wt.%) exhibited more uniform elemental distribution and lower porosity. Carbon values should be interpreted qualitatively. Further phase analysis by XRD is recommended.

Economic feasibility, under the conditions evaluated, thermite welding costs 290 THB/joint versus SMAW (960 THB/joint), showing a 69.8% lower cost, with a Cost Ratio (CR) of 3.31. It requires only 15–20 minutes versus 90 minutes per joint, giving a Time Reduction Ratio (TRR) of 4.5, equivalent to approximately 24 joints per 8-hour shift compared with 5–6 joints using SMAW. These results suggest promising economic performance and operational efficiency for field rail maintenance applications. A comprehensive lifecycle cost analysis is recommended for full economic validation.

The hardness results showed that Mold Type 2 provided more uniform hardness values closer to those of the original rail material, with HAZ hardness of approximately 360–410 HV and weld zone hardness of approximately 320–360 HV. In contrast, Mold Type 1 exhibited higher and more fluctuating HAZ hardness values (395–476 HV). These results agree with the SEM and EDX analyses, which indicated that Mold Type 2 possessed a finer pearlitic structure and more uniform elemental distribution, making it more suitable for railway rail surface repair applications.

Acknowledgments

The research team gratefully acknowledges financial support from Phetchabun Rajabhat University, and technical support from the Program of Industrial Engineering Technology and Logistics, Faculty of Agricultural and Industrial Technology, Phetchabun Rajabhat University; the Faculty of Engineering, Rajamangala University of Technology Lanna Phitsanulok; the Faculty of Engineering and the Faculty of Technical Education, Rajamangala University of Technology Isan Khon Kaen Campus, for providing instruments and equipment for this research. Special thanks are extended to Mr. Pichai Wattanasrimongkol, Track Maintenance Supervisory Engineer, Khon Kaen District, State Railway of Thailand, and Assoc. Prof. Dr. Pharpas Mueangchanburi, Department of Mining and Materials Engineering, Faculty of Engineering, Prince of Songkla University, for expert consultation on rail material data and experimental data analysis.

Author Contributions

T.K.: Conceptualization, methodology, experimental design, development of the thermite welding procedure and mold preparation plan, coordination of experimental implementation, data collection and organization, formal analysis of mold properties, weld characteristics, microstructural results, hardness distribution, and economic feasibility, interpretation of experimental findings, development of the discussion and conclusions, project administration, and corresponding author responsibility; P.D.: Conceptualization, methodology, experimental procedure development, welding and metallurgical interpretation, data collection, formal analysis, interpretation of hardness and microstructural results, discussion of findings, conclusion development, co-writing—original draft preparation, writing—review and editing, supervision, and writing—original draft preparation; C.R.: Investigation, resources, compressive strength testing of sand mold specimens, provision of materials-testing expertise, consultation on testing protocols for mold property characterization, validation of mold-related experimental data, interpretation of mold performance and suitability for thermite welding applications, and writing—review and editing; N.S.: Investigation, preparation of rail specimens and experimental materials, Vickers hardness testing of repaired rail specimens, hardness data collection, data organization, and contribution to the interpretation of hardness distribution in the repaired rail region; S.C.: Formal analysis, interpretation of experimental results, discussion of findings, technical review of the manuscript, and contribution to manuscript revision and editing. All authors have read and approved the final manuscript.

Conflicts of Interest

The authors declare no conflict of interest.

Declaration of generative AI and AI-assisted technologies in the writing process

The authors utilized the ChatGPT tool to enhance the language and readability of the manuscript.

References

[1] W. Lahamornchaiyakul, S. Chuenchomnakjad, T. Khrueaphue, and P. Dhinnabutra, "Finite element simulation of surface repair welding of grade R260 railway rails using thermite welding," *Journal of Metals, Materials and Minerals*, vol. 36, no. 2, pp. 1-10, 2026, doi:10.55713/jmmm.v36i2.2508.

[2] A. Ekberg and E. Kabo, "Fatigue of railway wheels and rails under rolling contact and thermal loading—An overview," *Wear*, vol. 258, no. 7–8, pp. 1288–1300, 2005, doi: 10.1016/j.wear.2004.03.039.

[3] I. I. Ekanem, A. E. Ikpe, and N. E. Itiat, "Overview of thermit welding process for railway applications: A mixture of iron oxide and aluminium powder joining techniques," *Journal of Materials and Manufacturing Technology*, vol. 1, no. 1, pp. 66–79, 2024, doi: 10.48314/jmmt.v1i1.28.

[4] B. Andersson, E. Steyn, M. Ekh, and L. Josefson, "Simulation-based assessment of railhead repair welding process parameters," *Welding in the World*, vol. 69, pp. 177–197, 2025, doi: 10.1007/s40194-024-01837-y.

[5] K. Saita and K. Kariminek, M. Ueda, K. Iwano, T. Yamamoto, and K. Hiroguchi, "Trends in rail welding technologies and our future approach," *Nippon Steel & Sumitomo Metal Technical Report*, no. 105, pp. 84–92, 2013.

[6] Y. Chen, F. V. Lawrence, C. P. L. Barkan, and J. A. Dantzig, "Heat transfer modelling of rail thermite welding," in *Proceedings of the Institution of Mechanical Engineers, Part F: Journal of Rail and Rapid Transit*, vol. 220, no. 3, pp. 207–217, 2006, doi: 10.1243/09544097F01505.

[7] V. Reddy, G. Chattopadhyay, P.-O. Larsson-Kråik, and D. J. Hargreaves, "Modelling and analysis of rail maintenance cost," *International Journal of Production Economics*, vol. 105, no. 2, pp. 475–482, 2007, doi: 10.1016/j.ijpe.2006. 04.007.

[8] K. V. Redkin, C. I. Garcia, A. J. DeArdo, D. Gutscher, and S. Kalay, "Microstructural analysis of thermite welds," in *Proceedings of the ASME 2010 Rail Transportation Division Fall Technical Conference*, 2010, pp. 1–8, doi: 10.1115/RTDF2010-42001.

[9] A. R. Khan, Y. Xu, X. Wang, C. Han, and C. Li, "Effect of cooling rate on microstructure and mechanical properties in the CGHAZ of electroslag welded pearlitic rail steel," *Metals*, vol. 9, no. 7, Art. no. 742, 2019, doi: 10.3390/met9070742.

[10] R. Gehrmann, P. Radmann, and J. Keichel, "Optimization of thermit welding," in *Proceedings of the 10th International Heavy Haul Association Conference*, New Delhi, India, 2013.

[11] M. A. Swartz, T. J. Wooley, and R. H. Kachik, "Method and mold for aluminothermic welding of rails," U.S. Patent 5 215 139, Jun. 1, 1993.

[12] T. Voigt, M. Schöne, M. Kohlhase, O. Nelles, and M. Kuhn, "Using design of experiments to support the commissioning of industrial assembly processes," in *Intelligent Data Engineering and Automated Learning – IDEAL 2022*, H. Yin et al., Eds. Cham: Springer, 2022, pp. 379–390, doi: 10.1007/978-3-031-21753-137.

[13] P. Sripraya and C. Saikaew, "Improving quality of recycled plastic products," *Engineering and Applied Science Research*, vol. 36, no. 2, pp. 87–95, 2009.

[14] G. Lucchetta, P. F. Bariani, and W. A. Knight, "A new approach to the optimization of blends composition in injection moulding of recycled polymers," *CIRP Annals - Manufacturing Technology*, vol. 55, no. 1, pp. 465–468, 2006, doi: 10.1016/S0007-8506(07)60460-0.

[15] Y. Chen, F. V. Lawrence, C. P. L. Barkan, and J. A. Dantzig, "Weld defect formation in rail thermite welds," in *Proceedings of the Institution of Mechanical Engineers, Part F: Journal of Rail and Rapid Transit*, vol. 220, no. 4, pp. 373–384, 2006, doi: 10.1243/0954409JRRT44.

[16] R. Burapa, H. Z. Oo, W. Sangwiman, and P. Muangjunburee, "Influences of preheating parameters on the quality of weld by thermite rail welding," *Materials Research Express*, vol. 11, no. 6, Art. no. 066507, 2024, doi: 10.1088/2053-1591/ad51db.

[17] P. J. Mutton and E. F. Alvarez, "Failure modes in aluminothermic rail welds under high axle load conditions," *Engineering Failure Analysis*, vol. 11, no. 2, pp. 151–166, 2004, doi: 10.1016/j.engfailanal.2003.05.003.

[18] S. Weiss, I. Riehl, J. Hantusch, and U. Gross, "Numerical investigation on the crucible discharge of steel and slag during the aluminothermic welding process," *Archives of Metallurgy and Materials*, vol. 63, no. 1, pp. 173–180, 2018, doi: 10.24425/118925.

[19] R. G. Kewalramani, I. Riehl, J. Hantusch, and T. Fieback, "Numerical investigation of the cooling stage during aluminothermic welding of rails: Rapid welding process without preheating," *Thermal Science and Engineering Progress*, vol. 37, Art. no. 101610, 2023, doi: 10.1016/j.tsep.2022.101610.

[20] T. A. Patel and V. Badheka, "Rail welding technology: Processes and welding quality," in *Recent Advances in Mechanical Infrastructure*, P. M. George et al., Eds. Singapore: Springer, 2022, pp. 363–373, doi: 10.1007/978-981-16-7660-433.

[21] A. Guerrero, J. Belzunce, C. Betegón, J. Jorge, and F. J. Vigil, "Hot rolling process simulation: Application to UIC-60 rail rolling," *Recent Patents on Mechanical Engineering*, vol. 3, no. 1, pp. 65–71, 2010, doi: 10.2174/1874477X110 03010065.

[22] European Committee for Standardization, *Railway Applications - Track - Rail - Part 1: Vignole Railway Rails 46 kg/m and Above*, Standard EN 13674-1:2003, 2003.

[23] T. P. Leso, C. W. Siyasiya, R. J. Mostert, and J. Moema, "Study of rolling contact fatigue, rolling and sliding wear of class B wheel steels against R350HT and R260 rail steels under dry contact conditions using the twin disc setup," *Tribology International*, vol. 174, Art. no. 107711, 2022, doi: 10.1016/j.triboint.2022.107711.

[24] V. Lafilé, J. Marteau, M. Risbet, S. Bouvier, P. Merino, and A. Saulot, "Characterization of the microstructure changes induced by a rolling contact bench reproducing wheel/rail contact on a pearlitic steel," *Metals*, vol. 12, no. 5, Art. no. 745, 2022, doi: 10.3390/met12050745.

[25] L. Josefson, R. Bisschop, M. Messaadi, and J. Ringsberg, "Residual stresses in thermite welded rails: Significance of additional forging," *Welding in the World*, vol. 64, no. 7, pp. 1195–1212, 2020, doi: 10.1007/s40194-020-00912-4.

[26] W. J. Hui, Z. B. Xu, Y. J. Zhang, X. L. Zhao, C. W. Shao, and Y. Q. Weng, "Hydrogen embrittlement behavior of high strength rail steels: A comparison between pearlitic and bainitic microstructures," *Materials Science and Engineering: A*, vol. 704, pp. 199–206, 2017, doi: 10.1016/j.msea.2017.08.022.

[27] J. Goldak and M. Akhlaghi, *Computational Welding Mechanics*. New York, NY, USA: Springer, 2005.

[28] L. C. Schroeder and D. R. Poirier, "The mechanical properties of thermite welds in premium alloy rails," *Materials Science and Engineering: A*, vol. 63, no. 1, pp. 1–21, 1984, doi: 10.1016/0025-5416(84)90159-9.

[29] European Committee for Standardization, *Railway Applications - Track - Aluminothermic Welding of Rails - Part 1: Approval of Welding Processes*, Standard EN 14730-1:2006, 2006.

[30] H. Aglan and T. Rahman, "Effect of preheating temperature and cooling rate on the

microstructure development of welded pearlitic rail steel," *Microscopy and Microanalysis*, vol. 26, suppl. 2, pp. 2662–2663, 2020, doi: 10.1017/S1431927620022357.

[31] C. Meric, E. Atik, and S. Sahin, "Mechanical and metallurgical properties of welding zone in rail welded via thermite process," *Science and Technology of Welding and Joining*, vol. 7, no. 3, pp. 172–176, 2002, doi: 10.1179/136217102225003702.

[32] ASTM International, *Standard Test Method for Compressive Strength of Hydraulic Cement Mortars*, ASTM Standard C109/C109M-21, West Conshohocken, PA, USA, 2021.

[33] N. Ilić, M. T. Jovanović, M. Todorović, M. Trtanj, and P. Šaponjić, "Microstructural and mechanical characterization of postweld heat-treated thermite weld in rails," *Materials Characterization*, vol. 43, no. 4, pp. 243–250, 1999, doi: 10.1016/S1044-5803(99)00006-6.

[34] T. Lesage, M.-N. Avettand-Fènoël, M. Masquelier, F. Danoix, and L. Kamgaing, "Consequences of thermite welding on the microstructure of the heat affected zone of a carbide-free bainitic steel rail," *Journal of Manufacturing Processes*, vol. 108, pp. 746–763, 2023, doi: 10.1016/j.jmapro.2023.11.027.

[35] Y. Liu, K. S. Tsang, E. T. Zhi'En, N. A. Subramaniam, and J. H. L. Pang, "Investigation on material characteristics and fatigue crack behavior of thermite welded rail joint," *Construction and Building Materials*, vol. 276, Art. no. 122249, 2021, doi: 10.1016/j.conbuildmat.2021.122249.

[36] S. Maya-Johnson, A. J. Ramirez, and A. Toro, "Fatigue crack growth rate of two pearlitic rail steels," *Engineering Fracture Mechanics*, vol. 138, pp. 63–72, 2015, doi: 10.1016/j.engfracmech.2015.03.023.

[37] Department of Rail Transport, "Thailand Rail Transport Development Plan 2022–2037," Ministry of Transport, Bangkok, Thailand, 2022. [Online]. Available: https://www.drt.go.th

[38] O. Buthphorm, V. Sukhotu, and T. Hengsadeekul, "An analysis of the development factors of rail freight transport in Thailand: A structural equation modeling approach," *Infrastructures*, vol. 9, no. 7, Art. no. 102, 2024, doi: 10.3390/infrastructures9070102.

[39] T. Nakpradit and B. Poopat, "Investigation of diffusible hydrogen content and microstructure examination of underwater welding," *Applied Science and Engineering Progress*, vol. 3, no. 3, pp. 45–51, 2013.

[40] G. T. Fry and F. V. Lawrence, "Modified thermite rail welding procedure," *Transportation Research Record*, no. 1470, pp. 93–98, 1994.

[41] Z. Hein and P. Muangjunburee, "Improving microstructure and hardness of softening area at HAZ of thermite welding on rail running surface," *Materials Today Communications*, vol. 34, Art. no. 105485, 2023, doi: 10.1016/j.mtcomm.2023.105485.

[42] A. Zoeteman, "Life cycle cost analysis for managing rail infrastructure: Concept of a decision support system for railway design and maintenance," *European Journal of Transport and Infrastructure Research*, vol. 1, no. 4, pp. 391–413, 2001, doi: 10.18757/ejtir.2001.1.4.3506.

[43] M. Sasidharan, M. P. N. Burrow, and G. H. Ghataora, "A whole life cycle approach under uncertainty for economically justifiable ballasted railway track maintenance," *Research in Transportation Economics*, vol. 80, Art. no. 100815, 2020, doi: 10.1016/j.retrec.2020.100815.